[1]G. L. Pearson and J. Bardeen, Phys. Rev. 75, 865 (1949).
[2]N. F. Mott, Phil. Mag. 6, 287 (1961).
[3]J. B. Krieger, Phys. Rev. 178, 1337 (1969).
[4]H. Brooks, Advan. Electron. Electron Phys. 7, 85 (1955); Phys. Rev. 83, 879 (1951).
[5]V. I. Fistul, E. M. Omelyanovsky, D. G. Andrianov, and I. V. Dakhovskii, in *Proceedings of the Seventh International Conference on the Physics of Semiconductors, Paris*, 1964 (Academic, New York, 1964), p. 371.
[6]P. W. Chapman, O. N. Tufte, J. D. Zook, and D. Long, J. Appl. Phys. 34, 3291 (1963).
[7]F. S. Ham, Phys. Rev. 100, 1251 (1955).
[8]R. Ito, J. Phys. Soc. Japan 18, 1604 (1963).
[9]C. Herring and E. Vogt, Phys. Rev. 101, 944 (1956); 105, 1933 (1957).
[10]A. G. Samoilovich, I. Ya. Korenblit, and I. V. Dakhovskii, Dokl. Akad. Nauk SSSR 139, 355 (1961)[Soviet Phys. Doklady 6, 606 (1962)].
[11]B. Abeles and S. Meiboom, Phys. Rev. 95, 31 (1954).
[12]P. J. Price, Phys. Rev. 104, 1223 (1956).
[13]M. J. Katz, Phys. Rev. 140, A1323 (1965).
[14]J. M. Ziman, *Electrons and Phonons* (Oxford U. P., London, 1960), p. 275.
[15]E. J. Moore and H. Ehrenreich, Solid State Commun. 4, 407 (1966).
[16]E. J. Moore, Phys. Rev. 160, 607 (1967); 160 618 (1967); Harvard University Technical Report No. ARPA-24, 1966 (unpublished).
[17]T. Meeks, J. B. Krieger, and E. Esposito, Bull. Am. Phys. Soc. 15, 554 (1970); and (unpublished).
[18]J. B. Krieger and S. Strauss, Phys. Rev. 169, 674 (1968).
[19]J. Friedel, Phil. Mag. 43, 153 (1952).

PHYSICAL REVIEW B VOLUME 3, NUMBER 4 15 FEBRUARY 1971

Lattice Dynamics of Grey Tin and Indium Antimonide†

D. L. Price and J. M. Rowe
Solid State Science Division, Argonne National Laboratory, Argonne, Illinois 60439

and

R. M. Nicklow
Solid State Division, Oak Ridge National Laboratory, Oak Ridge, Tennessee 37830
(Received 18 September 1970)

We have measured the phonon-dispersion relations in symmetry directions for α-Sn at 90 °K and InSb at 300 °K. A limited number of measurements were made at 240 °K in α-Sn to look for effects associated with the phase transition, but none were found. The two dispersion relations are qualitatively similar, the main differences arising from the lower symmetry and a slight general drop in frequency in going from α-Sn to InSb. Systematic trends in the comparison with other group-IV and III-V semiconductors can be seen. We have found second-neighbor shell models which give a reasonable description of the dispersion relations but in which the parameters are poorly defined and apparently devoid of physical meaning. The microscopic implications of this fact are discussed.

I. INTRODUCTION

The horizontal sequence of covalent compounds centered on tin, together with tin itself in the semiconducting phase, provides a unique system for testing theories of covalently bonded crystals. InSb and CdTe form stable compounds in the zinc-blende structure with a lattice parameter nearly identical to that of α-Sn; γ-AgI also has a similar lattice parameter but is a metastable phase.[1] Grey tin itself has a zero direct band gap,[2] which has led to speculations[3] about a singularity in the dielectric function as $\vec{q} \to 0$ and a possible excitonic transition at low temperatures in highly pure material (Sherrington and Kohn, Ref. 4). Going outwards in the horizontal sequence, the band gap increases and the compounds become more ionic (Herman, Cardona, and Greenaway, Ref. 4). Phillips[5] has developed a microscopic theory of covalent bonding which leads to an ionicity scale[6] in which the ionic characters f_i of InSb, CdTe, and AgI are 0.32, 0.67, and 0.77, respectively; since $f_i = 0.785$ is taken to represent the boundary between octahedral and tetrahedral bonding, the observed polymorphism in AgI is consistent with this scale. A study of the lattice dynamics of the members of this sequence should reveal the effects of this increasing ionicity since the lattice structures and masses do not vary much. We present here measurements of phonon-dispersion curves in the first two members, α-Sn [7] and InSb.

Grey tin is also interesting because it undergoes at normal pressures the transition to a metallic state which InSb, CdTe, Ge, and Si exhibit only under pressure.[8] This aspect will not be discussed here, partly because it does not appear to be connected with the zero band gap[9] and also because no evidence for it was found in the temperature depen-

dence of the measured dispersion curves; the thermodynamic aspects of the transition have been covered in Ref. 7.

Phillips's microscopic theory establishes reasonably satisfactory connections with the trends in properties such as crystal structure and band gaps,[6] dielectric constant,[9] and cohesive energy.[10] Dynamical properties can be calculated by assuming that the bond charges are point charges constrained to lie at the midpoints of the bonds during the motion. Martin[11] has calculated the phonon-dispersion relation in silicon on this basis and obtained agreement with experiment to within 10% after minor adjustments to forms for the pseudopotential and dielectric function given in the literature. It is not, however, obvious how to extend the theory beyond the point bond-charge assumption, and predictions of dynamical effective charges[5] are less satisfactory than some of the other properties. On the other hand, more rigorous microscopic theories of the lattice dynamics of insulators[12-14] have established formulations without so far leading to any calculations of specific cases. Measured dispersion curves in covalently bonded materials have up to now therefore been interpreted with the use of phenomenological models. These have been based on the rigid-ion approximation, with either interatomic[15] or valence force-field[16] short-range forces, or on the dipolar approximation, such as the shell model introduced by Dick and Overhauser and other theories more or less equivalent.[17] The rigid-ion models are definitely unsuitable in view of the large electronic polarizabilities of these materials, while the application of point-dipole models, with the concomitant Lorentz form for the local field, to materials with extended valence charge distributions is also questionable.[18] However, it was suggested by Cochran[19] that the form of the shell-model equations might have a more general validity than the literal shell-model interpretation, and Sinha[12] has shown rigorously that one can achieve this generalization by defining form factors for the shells; the shell-model equations are then applicable under a dipolar approximation that is only exact in the tight-binding limit, but may still be a reasonable approximation in other cases.

The shell model, in the form proposed by Cochran[20] for Ge and extended to second-neighbor short-range forces by Dolling,[21] has the advantage for our purposes in that it has been used to interpret similar neutron data in diamond,[22,23] Si,[21] Ge,[23,24] GaAs,[25] and GaP,[26] and so the parameters fitted can be directly compared. In view of the above discussion, however, one should not expect the parameters describing the short-range forces in terms of first- and second-neighbor interactions to have much physical significance.

II. EXPERIMENTS

The α-Sn crystal was grown from a mercury amalgam[27] by Ewald of Northwestern University, and had a volume of about 0.5 cm^3. On the basis of previous experience with similar crystals it was expected to have about 10^{16} carriers/cm^3, and also to have small occlusions of mercury. The crystal was kept below 273 °K prior to, and during, the measurement, to avoid the diffusion of these through the crystal and also to prevent transformation to the β phase. Chemical analysis after the experiment showed a total mercury content of 0.16% of the weight of the crystal, with traces of other elements.

Three single-crystal slabs were used for the InSb measurements, obtained from Asarco Intermetallics Corp. Because of the high-absorption cross section of In (190 b for thermal neutrons), the slabs were cut with a thickness of 0.3 cm, about one mean free path, and aligned side by side to cover an area about 2.5 by 5 cm. The material was n type, and mobility and resistivity were given as 5.53×10^5 cm^2/V sec and 0.169 Ω cm, respectively, at 77 °K, indicating a donor concentration of about $8\times10^{13}/cm^3$. Thus the phonon-plasmon coupling seen, for example, by neutrons in PbTe[28] and by Raman scattering in GaAS[29] should not be observable in these crystals. In both experiments the crystals were mounted on plates covered with neutron-absorbing material, with the [001] axis normal to the plate and oriented with the $(1\bar{1}0)$ plane in the plane of the spectrometer. We did not, therefore, measure the modes propagating along [110] and polarized along $[1\bar{1}0]$. Both sets of crystals appeared to be highly perfect with mosaic spreads well under the instrumental collimation of 20 min.

The experiments were carried out with the three-axis spectrometer[30] at the High-Flux Isotopes Reactor at Oak Ridge. Because of the small sample size in the case of α-Sn and the small effective size (due to absorption) in the case of InSb, and also because of the relatively low inelastic cross section due to the high masses, the measurements were very difficult, even at a high-flux reactor. Be crystals cut along the (0002) and $(10\bar{2}1)$ planes were used for monochromators in the two experiments, and a (0002) Be crystal was used for analyzer in both. The constant-Q technique was used throughout the measurements, with fixed analyzer energy; this was set to 3.8, 7.5, 9.9, or 10.4 THz, depending on the energy and momentum transfer involved.

Preliminary models were used before the measurements to calculate phonon structure factors for different positions in reciprocal space. The fact that both samples were backed on absorbing plates often prevented us from measuring a phonon

at a point where the structure factor would be optimized, especially when the polarization vectors had large components along the [110] direction, which was along the surface of the plate. The InSb structure factors are slightly different from those for α-Sn; first, because two atoms with different scattering lengths are involved and, second, because the zinc-blende structure has lower symmetry than the diamond. It turned out that neither of these two effects altered the optimal point in reciprocal space for measuring any particular mode, although the reduced symmetry complicated the measurements in a number of cases, as discussed in Sec. III. We were, however, forced to measure some modes at different points in the InSb experiment because of the high absorption, which led to low intensities whenever either incident or scattered beam tended to be parallel to the crystal surface.

The principal α-Sn measurements were made at 90 °K; a number of measurements were made at 240 °K to look for effects associated with the phase transition,[7] but no frequency changes outside the experimental error of the 90 °K measurement were observed. There was a slight average decrease in frequency (< 1%), consistent with the values reported for frequency shifts in Ge.[24] For this reason, and for convenience in handling the bulky sample assembly, the InSb measurements were performed at room temperature, 300 °K.

III. RESULTS

The measured phonon frequencies with estimated errors (about 95% confidence limits) are listed in Table I, and the measured dispersion curves for the two materials are shown by the symbols in Figs. 1 and 2. The continuous curves represent shell-model fits, discussed in Sec. VI. In the figures the errors are indicated by bars wherever they are larger than the size of the points. It is immediately apparent that the two dispersion relations are qualitatively similar, the main differences being dictated by the lower symmetry of the zinc-blende structure compared with the diamond.[31] For the modes measured, the important differences in going to InSb from α-Sn are as follows.

TABLE I. Phonon frequencies in α-Sn(90 °K) and InSb(300 °K). Frequency (THz) vs reduced wave vector. $\zeta = aq/2\pi$.

[00ζ]

ζ	α-Sn $\Delta_5(A)$	InSb $\Delta_3(A)$	α-Sn Δ_1	InSb $\Delta_1(A)$	α-Sn Δ_2'	InSb $\Delta_1(0)$	α-Sn $\Delta_5(0)$	InSb $\Delta_3(0)$
0.0					6.00 ± 0.06	5.90 ± 0.25	6.00 ± 0.06	5.54 ± 0.05
0.2	0.675 ± 0.01	0.58 ± 0.03	1.12 ± 0.04	1.07 ± 0.02	5.93 ± 0.07	5.70 ± 0.15	5.78 ± 0.12	5.40 ± 0.20
0.4	1.15 ± 0.03	1.02 ± 0.03	2.05 ± 0.08	2.05 ± 0.02	5.82 ± 0.10	5.56 ± 0.10	5.61 ± 0.12	5.22 ± 0.12
0.6	1.29 ± 0.03	1.20 ± 0.04	3.07 ± 0.06	2.90 ± 0.06	5.51 ± 0.06	5.28 ± 0.08	5.55 ± 0.09	
0.8	1.30 ± 0.05	1.13 ± 0.05	3.93 ± 0.05	3.76 ± 0.06	5.14 ± 0.07	5.05 ± 0.10	5.54 ± 0.10	
1.0	1.25 ± 0.06	1.12 ± 0.05	4.67 ± 0.06	4.30 ± 0.10	4.67 ± 0.06	4.75 ± 0.20	5.51 ± 0.08	5.38 ± 0.17

[$\zeta\zeta\zeta$]

ζ	α-Sn $\Lambda_3(A)$	InSb	α-Sn $\Lambda_1(A)$	InSb	α-Sn $\Lambda_1(0)$	InSb	α-Sn $\Lambda_3(0)$	InSb
0.0					6.00 ± 0.06	5.90 ± 0.25	6.00 ± 0.06	5.54 ± 0.05
0.1	0.50 ± 0.02	0.46 ± 0.01	1.06 ± 0.015	1.03 ± 0.02	5.91 ± 0.10	5.62 ± 0.15	5.88 ± 0.08	5.38 ± 0.10
0.2	0.84 ± 0.03	0.80 ± 0.04	2.08 ± 0.04	1.98 ± 0.04	5.68 ± 0.09	5.56 ± 0.08	5.79 ± 0.11	5.39 ± 0.11
0.3	0.96 ± 0.03	0.93 ± 0.04	2.91 ± 0.04	2.83 ± 0.05	5.50 ± 0.08	5.24 ± 0.10	5.77 ± 0.07	5.34 ± 0.07
0.4	0.99 ± 0.04	0.98 ± 0.05	3.72 ± 0.04	3.43 ± 0.06	5.17 ± 0.06	4.94 ± 0.13	5.78 ± 0.07	5.28 ± 0.07
0.5	1.00 ± 0.04	0.98 ± 0.05	4.15 ± 0.04	3.81 ± 0.06	4.89 ± 0.08	4.82 ± 0.10	5.74 ± 0.12	5.31 ± 0.06

[$\zeta\zeta$0]

ζ	α-Sn $\Sigma_3(A)$	InSb $\Sigma_1(A)$	α-Sn $\Sigma_1(A)$	InSb $\Sigma_1(2)$	α-Sn $\Sigma_3(0)$	InSb $\Sigma_1(3)$	α-Sn $\Sigma_1(0)$	InSb $\Sigma_1(4)$
0.0					6.00 ± 0.06	5.54 ± 0.05	6.00 ± 0.06	5.90 ± 0.25
0.15	0.75 ± 0.01		1.20 ± 0.06					
0.2	0.99 ± 0.01	0.92 ± 0.01	1.61 ± 0.04	1.58 ± 0.05		5.32 ± 0.08[a]	5.93 ± 0.10	5.32 ± 0.08[a]
0.4	1.63 ± 0.02	1.525 ± 0.01	2.74 ± 0.03	2.73 ± 0.03	5.23 ± 0.09		5.84 ± 0.08	5.40 ± 0.07
0.6	1.96 ± 0.05	1.82 ± 0.02	3.61 ± 0.03	3.46 ± 0.05	4.73 ± 0.05	4.57 ± 0.07	5.78 ± 0.11	5.38 ± 0.10
0.8	1.74 ± 0.04	1.62 ± 0.04	4.33 ± 0.05	4.08 ± 0.06	4.34 ± 0.08	4.22 ± 0.10	5.54 ± 0.09	5.55 ± 0.15
1.0	1.25 ± 0.06	1.12 ± 0.05	4.67 ± 0.06	4.30 ± 0.10	4.67 ± 0.06	4.75 ± 0.20	5.51 ± 0.08	5.38 ± 0.17

[a]This value could contain contributions from either or both branches.

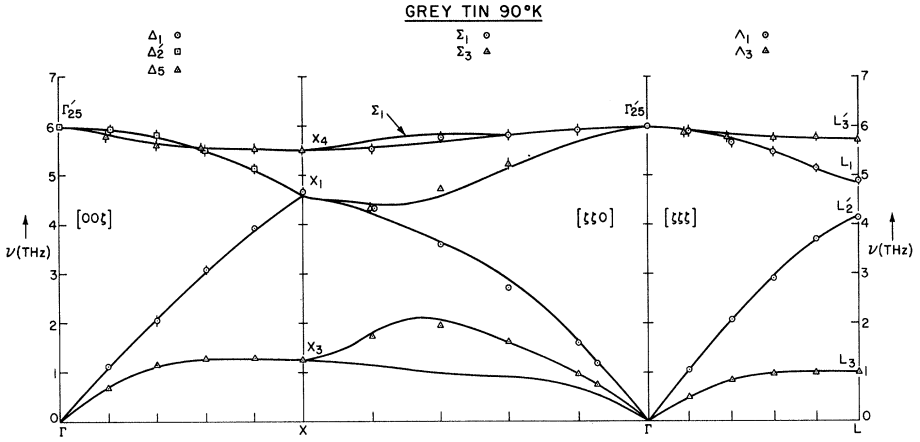

FIG. 1. Dispersion relation for α-Sn at 90 °K. The symbols represent measured frequencies and the solid lines shell-model calculations.

A. $X_1 \rightarrow X_1 + X_3$

The longitudinal modes at the zone boundary in the [100] direction are ones in which only one atom in the unit cell is moving. These are no longer degenerate if there are two types of atom. Since the scattering lengths for In and Sb are rather similar, the structure factors for the two modes in InSb are also similar and it is difficult to identify them on grounds of intensity. The data points in Fig. 2 are therefore denoted by a joint mode label. They are derived from a neutron group in which the two modes are barely resolved, since the frequencies are closer than the resolution of the instrument, which varied from 0.5 to 1.0 THz for all but the low acoustic modes.

B. $\Gamma'_{25} \rightarrow \Gamma_{15}(L) + \Gamma_{15}(T)$

The presence of two types of atom causes a coupling of the long-wavelength vibrations to the macroscopic electric field. This can arise either from a difference in the charges of the two ions or from a difference in the polarizabilities. The effect of the coupling is to increase the limiting frequency of the longitudinal mode over that of the transverse as $\vec{q} \rightarrow 0$ along a particular direction. A neutron measurement at a forbidden reciprocal-lattice point yields contributions from both types of mode, depending on the shape of the resolution function in reciprocal space. Usually the transverse mode is favored because the resolution function tends to be more elongated perpendicular to $\vec{Q}$ than parallel to it, and the neutron picks out the components of polarization parallel to $\vec{Q}$. The value shown in Fig. 2 for the longitudinal mode is estimated on the basis of what are undoubtedly unresolved compound peaks, together with extrapolation from the modes measured at nonzero values of $\vec{q}$, and a suitably large error is assigned. Because of the low intensities caused by the high absorption, we were not able to cut down the vertical collimation, a procedure which was found effective in the case of GaAs.[25]

C. $\Sigma_1 + \Sigma_3 \rightarrow \Sigma_1$

In the case of α-Sn, the modes propagating in the [110] direction polarized in the $(1\bar{1}0)$ plane belong to two representations of the space group. Two modes belong to each representation, a fact which helps to distinguish the optic modes, as can be seen from Fig. 1. In InSb the higher frequency of the longitudinal mode at Γ would cause a crossing if

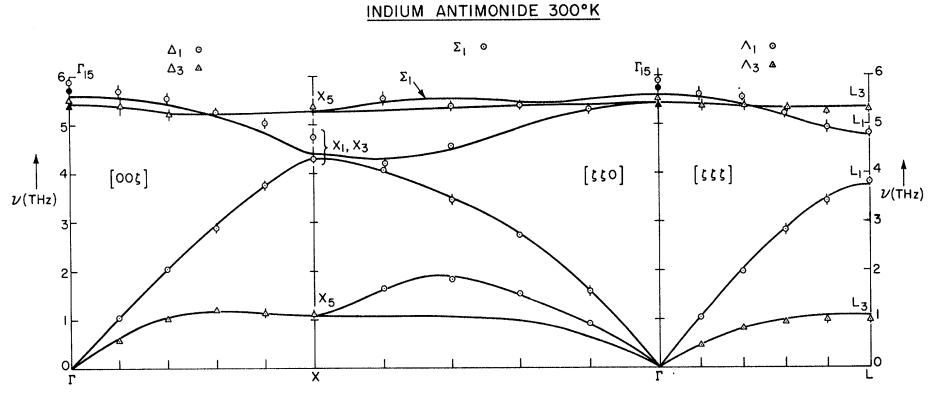

FIG. 2. Dispersion relation for InSb at 300 °K. The open symbols represent neutron measurements and the two closed symbols optical measurements (Refs. 36 and 43); the solid lines refer to shell-model calculations.

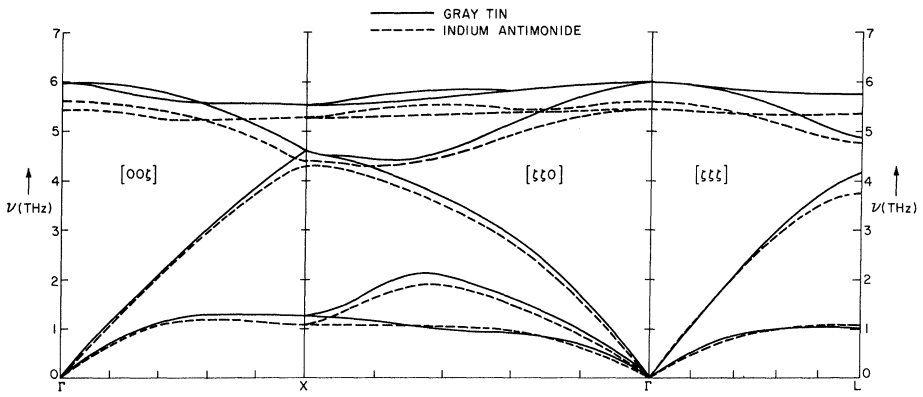

FIG. 3. Dispersion relations for α-Sn (solid lines) and InSb (dashed lines) derived from shell-model calculations.

the modes remained uncoupled. The lower symmetry, however, means that all four modes belong to the same representation and therefore repel each other instead of crossing. Measurements of modes near the repulsion region, such as our measurement of the optic mode at $\zeta = 0.2$, can therefore contain contributions from both modes and cannot be assigned to either one.

The longitudinal modes at the zone boundary in the [111] direction are nondegenerate in both structures. In α-Sn these belong to different representations, and it is found[32] that the acoustic mode belongs to L_2'. In InSb, they belong to the same representation but the physical situation is the same: Nearest neighbors along the propagation direction vibrate *in phase* in the acoustic mode.[31] The separation is greater, however.

Apart from these details, the dispersion curves in the two materials are rather similar. In Fig. 3, we have transposed the curves from the two shell-model fits onto the same graph, showing the α-Sn with continuous lines and the InSb with dashed ones. It can be seen that the InSb curves tend to be lower, but by different amounts in different branches. This cannot be explained by differences in temperature, mass, or lattice spacing, which can only lead to effects less than 1%. A similar behavior has been observed for Ge and GaAs.[25]

It is also interesting to compare the results with the other semiconductors formed from elements of the same columns of the Periodic Table. The observed frequencies can be scaled by the appropriate ion plasma frequency given by

$$\overline{\nu}_p^2 = Z_1 Z_2 e^2/\pi \overline{M}\,\Omega\,,$$

where $Z_{1,2}$ are the valences, $\overline{M}$ is the reduced mass given by $\overline{M}^{-1} = M_1^{-1} + M_2^{-1}$, and Ω is the volume of the unit cell. Figure 4 shows the measured frequencies at high-symmetry points in diamond,[22] Si,[21] Ge,[24] and α-Sn, scaled in this way, and Fig. 5 shows similar results for BN,[33] AlP,[34] GaAs,[25,35] and InSb[36]; for the III-V compounds we use the first-order Raman data for the optic modes at Γ and the neutron data (which only exist for GaAs and InSb) for the other modes. If the dynamics could be described by Coulomb interactions between the positive ions embedded in a uniform negative charge, the scaled frequencies would be constant across the series (for the III-V compounds this is only exactly true for the long-wavelength optic frequencies). The variations can therefore be ascribed to varying behavior in the valence electrons. It can be seen that in both figures the longitudinal frequencies remain relatively constant, whereas the transverse optic go up and the transverse acoustic down, as one goes down the Periodic Table. One might expect the longitudinal modes to be mainly dependent on the density of valence electrons (taken care of by the scaling) and the transverse modes to be more sensitive to their detailed behavior. It has been noted[37,16] that the shear elastic moduli in these semiconductors also show more variation than the bulk moduli.

IV. OTHER EXPERIMENTAL DATA

The difficulties of preparing and working with single crystals of α-Sn have so far discouraged

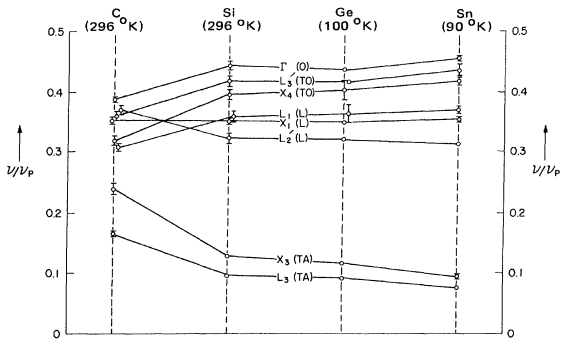

FIG. 4. Frequencies measured at high-symmetry points in C (diamond), Si, Ge, and α-Sn scaled by the ion plasma frequency.

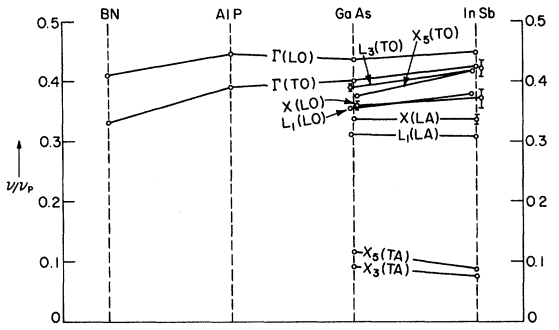

FIG. 5. Frequencies measured at high-symmetry points in BN, AlP, GaAs, and InSb, scaled by the ion plasma frequency.

measurements of its elastic constants. The dielectric constant, however, has been measured with an infrared reflectance method by Lindquist and Ewald,[38] who extrapolated measurements at long wavelengths, about 15 μ, to zero wavelength in order to correct for the effects of free carriers and obtained $\epsilon_0 = 24$. The vanishing band gap[2] leads to an additional interband contribution to the *static* dielectric constant from states close to the band edge. In the random-phase approximation this goes to infinity[3] like $1/q$ as $\vec{q} \to 0$, but when the impurity carriers are considered,[39] it leads instead to a contribution that is finite for all q but has a value that depends on the concentration. Because an optical wavelength of 15 μ implies a frequency of 20 THz, which is still considerably higher than the lattice frequencies, it is possible that a value of ϵ_0 greater than 24 would be appropriate for the lattice dynamics. We will, however, use this value both because of lack of other experimental data and because the validity of the random-phase approximation in this context has been questioned.[40] There is also, of course, an intraband contribution due to the free carriers, but it has been shown both theoretically[28] and experimentally[41] that this does not have any significant effect on the lattice dynamics of group-IV semiconductors.

There is a considerable amount of information on the long-wavelength properties of InSb. There have been several ultrasonic measurements[42] of the elastic constants as a function of temperature, and the two measurements with waves in the megacycle range are in good agreement. The long-wavelength transverse and longitudinal optic frequencies have been measured by a number of methods.[43] The most reliable results appear to be obtained either from studies of the infrared reflection spectrum or transmission spectrum through thin layers, or from first-order Raman scattering. Three infrared measurements[43] at 300 °K all give results in the range

$$\nu_{TO} = 5.39 \pm 0.02\,, \quad \nu_{LO} = 5.70 \pm 0.03 \text{ THz},$$

and first-order Raman scattering[36] gives

$$\nu_{TO} = 5.40\,, \quad \nu_{LO} = 5.73 \text{ THz}.$$

It can be seen from Table I that these are somewhat lower than our values; the discrepancy is within the error limits for the LO, but not the TO. These frequencies are marked by closed symbols in Fig. 2. It is interesting that infrared measurements at liquid helium temperature[44] give

$$\nu_{TO} = 5.54 \pm 0.09, \quad \nu_{LO} = 5.91 \pm 0.06 \text{ THz},$$

which agree fortuitously well with our 300 °K neutron measurements. The high-[45] and low-frequency dielectric constants ϵ_∞ and ϵ_0 can also be obtained from these studies. In practice, it is more accurate to obtain ϵ_∞ from index-of-refraction data and derive $(\epsilon_0 - \epsilon_\infty)$ from the reflectance measurements. Reference 44 gives $\epsilon_\infty = 15.68$ and $\epsilon_0 = 17.88$ at helium temperature, errors being about 0.1 in each case. The ratio of these is 1.14 ± 0.01, which implies that $\nu_{LO}/\nu_{TO} = 1.07$, from the Lyddane-Sachs-Teller relation. Our measurements give 1.065 ± 0.045 for this ratio, and the optical measurements give 1.06.

In principle, information about the frequencies of zone-boundary phonons can be obtained from the identification and measurement of critical points in second- and third-order infrared and Raman spectra. Frequencies in InSb derived in this way from infrared-transmission[46] and spectral-emission[47] studies are not entirely consistent either with each other or with the neutron data. The difficulties inherent in interpreting such data have been pointed out in connection with the group-IV semiconductors and GaAs,[23] and also with GaP.[22]

The coupling between the lattice vibrations and the electric field also has consequences for the elastic properties. The relation between the elastic stress and the macroscopic field in the zinc-blende structure is described by one piezoelectric constant e_{14}. The value of this constant has recently been measured for InSb and some other III-V compounds.[48] A related parameter is the internal strain constant γ_{14} which relates the change in relative position of the two atoms in the unit cell to the elastic strain; this can be measured with x rays. Measurements are not possible in III-V compounds, and have so far only been reported for Si and Ge,[49] but these values can be used as an extra test of the extent to which models for α-Sn and InSb are realistic. The coupling with the electric field also affects the elastic constants; in the zinc-blende structure the only constant involved is c_{44}, the value of which depends on whether it is measured at constant macroscopic field, effective field or displacement. In principle, this leads to different velocities for the shear modes governed by c_{44} in the [100] and [110] directions.[50] In practice, the difference in InSb is less than the experimental error of the neutron or ultrasonic

measurements; it would be significant, however, in a zinc-blende structure crystal which was tending to ferroelectricity.[50]

Finally, we should mention some published x-ray measurements[51] of phonon dispersion curves in InSb. Unfortunately, this method is indirect, involving measurements of absolute intensity which become even more difficult when there are two atoms in the unit cell. Limited measurements in the [100] and [111] directions at low temperatures are in reasonable agreement with our neutron data, but are less accurate. The room-temperature observations on the [100] longitudinal modes, however, showed anomalous effects which were explained by invoking plasmon-phonon coupling together with a dramatic drop in the frequency of the acoustic branch. We find no evidence of this in our measurements, and although the carrier concentration of the sample used in the x-ray measurements is not stated it is difficult to see how plasmon effects could affect the acoustic branch significantly.

V. SHELL MODEL

As stated in the Introduction, we have fitted the shell model developed by Cochran[20] and Dolling[21] to our data, in spite of the fact that not much physical significance can be attached to the values obtained. The advantages of this model are, first, that it has been used to interpret data in other group-IV and III-V semiconductors and, second, that it has sufficient generality to afford a description of all the available data. For example, the high-frequency dielectric constant ϵ_∞, and the fact that the piezoelectric constant is not completely described by the internal strains,[48] can both be explained in shell-model terms.

The model used corresponds to that introduced by Dolling and Waugh[25] for GaAs, and the notation is given in the Appendix. The ions are described by equal and opposite ionic charges and "atomic" and "mechanical" polarizabilities; the ion-ion, ion-shell, and shell-shell short-range interactions are described by first (α, β)- and second (λ, μ, ν, δ)-neighbor force constants, in which the suffixes R, T, and S denote the three types of interaction. For the group-IV crystals, the ionic charge is zero and the polarizabilities equal for the two atoms in the unit cell. Since the shell charges are actually fictitious, the dipole moments developed on the ions being the real physical quantities, the description contains two redundant parameters, and one can take $\alpha_R = \alpha_T$ without loss of generality. To reduce the number of parameters, the following further assumptions are made: (i) For the III-V compounds, the (III ion, V shell) and (III shell, V ion) short-range interactions are equal.[52] (ii) For the second neighbors, the constants for the R, T, and S interactions are in the ratio $1:1:S_R$, where $S_R = \alpha_S/\alpha_R$. (iii) For the III-V compounds, the III-III and V-V interactions are identical. Explicitly,

$$\underline{D}(\mathrm{III},\ \mathrm{III}) = \underline{D}^*(\mathrm{V},\ \mathrm{V}),$$

where $\underline{D}$ is $\underline{R}$, $\underline{T}$, or $\underline{S}$.

In the Appendix we give the expression for the dynamical matrix in terms of these parameters. We also give expressions for the other physical properties discussed in Sec. IV. These have been worked out for the zinc-blende structure by Cowley[53] using the perturbation procedures developed by Born and Huang.[54] He has invoked the approximation $\gamma_R = \gamma_T$ to simplify the expressions for e_{14} and c_{44}; we give the exact expressions which in general give significantly different results.[55]

VI. LEAST-SQUARES FITTING

A shell model fitted to the α-Sn neutron data and dielectric constant was presented in a previous paper. The fit to this model did not use the $\Sigma(110)$-direction data, except to determine the antisymmetric second-neighbor force constant δ. We have now included all the data and refined this model. A final value of $\chi^2 = 2.27$ was obtained. No other minima in the 11-dimensional parameter space were found, although extensive searches were made. We were also unable to obtain a fit by imposing any restrictions on the parameters (e.g., $\gamma_S = \gamma_T = \gamma_R$; $\alpha_S/\alpha_R = 1$). As previously noted, the full 11-parameter model did not converge properly to a well-defined minimum, and the covariance matrix indicated strong correlations between several of the parameters. The final values of the parameters were individually poorly determined, and some parameters have seemingly unphysical values (e.g., $\gamma_S = -7.0$). The final model gave a value for the dielectric constant ϵ_0 of 12, compared to an experimental value[38] of 24. As the value of χ^2 was very small we would, however, consider this model adequate for interpolation to unmeasured regions of reciprocal space.

For InSb, there are 14 parameters in the second-neighbor shell model described in Sec. V. We were able to find two separate minima in the 14-dimensional parameter space – one starting from the best values for the parameters found for α-Sn, the other starting from the best values for the parameters found for GaAs.[56] Neither minimum was well determined, and the two values of χ^2 found were, respectively, 3.18 and 2.03. In fitting these models, the experimental values of the elastic, dielectric, and piezoelectric constants (see Sec. IV) were used in addition to the neutron data. Varying the weights on these data by a factor of 10 made little change in the model parameters found. The values of χ^2 quoted above were obtained when the errors on the elastic and dielectric constants were

TABLE II. Observed and calculated elastic and dielectric properties.

Property	Units	α-Sn (90 °K)		InSb (300 °K)	
		Obs	Calc	Obs	Calc
c_{11}	10^{12} dyne/cm^2		0.690	0.6669 ± 0.007[d]	0.6555
c_{12}			0.293	0.3645 ± 0.004[d]	0.3936
c_{44}			0.362	0.3020 ± 0.002[d]	0.3082
ϵ_∞		24[a]	12.20	15.68 ± 0.1[e]	15.66
ϵ_0				17.88 ± 0.1[e]	16.74
ν_{TO}	THz	6.00 ± 0.06	5.97	5.54 ± 0.05; 5.40[f]	5.43
ν_{LO}				5.90 ± 0.25; 5.73[f]	5.61
e_{14}	10^4 esu/cm^2			−2.13 ± 0.2[g]	−2.02
ζ		0.64 ± 0.04[b]	0.67		0.70
a	Å	6.483[c]		6.4793[h]	
M	amu	118.70		114.82, 121.76	

[a]Reference 38.
[b]Value for Ge, Ref. 49.
[c]J. Thewlis and A. R. Davey, Nature 174, 1011 (1954).
[d]Reference 42.
[e]Reference 44.
[f]Reference 36.
[g]Reference 48.
[h]G. Gieseche and H. Pfister, Acta Cryst. 11, 369 (1958); S. I. Novikova, Fiz. Tverd. Tela 2, 2341 (1960) [Soviet Phys. Solid State 2, 2087 (1961)].

increased by a factor of 10 over the values given in Table II, and χ^2 thus reflects only the fit to the neutron data. The first model, started from α-Sn, fitted the neutron data for the optical branches quite well, giving less good agreement for the acoustic branches and non-neutron data. For the second model, started from GaAs, the converse was true. For both models convergence was very slow and incomplete, and the covariance matrix showed that the final values of the parameters were poorly determined and correlated, as in the α-Sn fit. In comparing fits, the larger errors assigned to the InSb data should be noted.

In Table II, we show the values of the elastic and dielectric properties calculated from the models and also the experimental data where these exist. We give results for the second InSb model, started from the GaAs parameters, in the figures and tables. In Table III, we show the values of the parameters of the models, and compare with the parameters of similar models fitted to diamond,[22,23] Si,[21] Ge,[23] GaAs,[57] and GaP[26]; the latter compound contains elements from different rows of the Periodic Table and is a less meaningful comparison. It is difficult to find any systematic trends in the values of the parameters, except perhaps an increase in γ_R, a decrease in γ_S (to large negative values), and a decrease in the antisymmetric force constant δ in going from C through to α-Sn and from GaAs to InSb. It is interesting that the fits for

TABLE III. Values of shell-model parameters fitted to group-IV and III-V crystals.

	C[a]	Si[b]	Ge[c]	α-Sn	GaP[d]	GaAs[e]	InSb
α_R	9.245	21.42	27.77	12.81	32.68	19.67	12.08
Z_1					0.31	−0.018	−0.061
π_1	0.0444	0.0401	0.0312	0.0841	0.0182	0.0754	0.0852
π_2					0.0119	0.0142	0.0685
d_1	0.432	1.199	1.372	0.695	1.277	1.588	0.677
d_2					0.990	0.714	0.823
S_R	3.342	1.364	1.262	0.953	1.173	1.267	1.491
γ_R	−0.092	0.214	0.242	0.352	0.335	0.222	0.577
γ_T	−1.198	−0.009	0.151	−0.880	0.215	0.043	0.226
γ_S	−1.198	−0.328	−0.017	−7.001	0.097	−0.133	−1.163
μ_R	1.205	−0.725	−1.651	0.048	−2.35	−0.815	0.055
λ_R	−0.413	−2.199	−2.880	0.115	−2.76	−1.941	−0.470
ν_R	2.035	0.818	0.209	1.256	−0.51	0.736	0.499
δ_R	4.75	1.70	2.00	1.048	2.14	0.55	0.534

[a]See Refs. 22 and 23.
[b]See Refs. 21 and 23.
[c]See Ref. 23.
[d]See Ref. 26.
[e]See Ref. 57.

GaAs and InSb both show Z_1 slightly negative, i.e., a small positive charge on the group-III ion. The calculated value of e_{14} in InSb is nevertheless negative, in agreement with experiment. This shows the importance of using the exact expression for e_{14}, since it would be positive if governed only by the internal strain.

Dispersion curves calculated from the fitted models are plotted in Figs. 1 and 2, along with the neutron data. It is seen that the α-Sn model gives a reasonable description of the measured dispersion curves, the major discrepancies being in the $\Sigma_3(A)$ and $\Sigma_1(0)$ branches in the [110] direction. The InSb model is a less satisfactory description, being especially poor for the whole $\Delta_1(0)$ branch in the [100] direction; this is presumably because of the low weights assigned to the LO modes at Γ and X, since the value of χ^2 is comparable to that found for the α-Sn model.

VII. CONCLUSIONS

The phonon dispersion relations in α-Sn and InSb have been found to be qualitatively very similar. The quantitative differences are the following: (i) a small splitting in InSb of modes which are required by symmetry to be degenerate in α-Sn, and (ii) a slight general lowering in frequency in going from α-Sn to InSb. Our measurements in α-Sn show no anomalous effects which can be associated either with the vanishing band gap or with the transition to the metallic phase at room temperature. In both materials, comparison with the semiconductors in the corresponding vertical sequences shows consistent changes in the frequencies of the transverse modes, whereas the longitudinal modes remain relatively constant when scaled with the appropriate ion plasma frequency.

Our attempts to quantify these trends have not been satisfactory. In fitting shell models to the neutron data and information on long-wavelength properties, we have come up with reasonable representations of the dispersion relations. However, the parameters of the models are poorly determined and highly correlated, and also some real discrepancies with the non-neutron data remain. Further, the parameters do not fall into any physically meaningful pattern. This last fact is elucidated by Sinha's[12] microscopic interpretation of the shell-model equation, in which the different kinds of short-range force constants are shown to be attempts to represent the q dependence of the polarizability and the ion form factors and pseudopotentials. Sinha also shows that the dipolar approximation on which the shell model is based becomes less valid as the valence-electron wave functions are extended and as the band gap decreases. The poorer performance of the shell model for such materials has also been noted experimentally.[28]

We hope that the detailed data presented for these two narrow-gap semiconductors, and the systematic trends noted for the vertical sequences of group-IV and III-V crystals, will stimulate a microscopic calculation of the lattice dynamics of these materials from first principles. The main task is to establish a satisfactory dielectric matrix. If the dipolar approximation as formulated by Sinha is then reasonably well satisfied, it is a simple matter to invert the matrix in closed form; otherwise one can invert the matrix by numerical methods. One can then adopt an appropriate pseudopotential and proceed to calculate the dynamical matrix in the prescribed manner.[13,14]

ACKNOWLEDGMENTS

Two of us (D. L. P. and J. M. R.) would like to thank Dr. D. Billington, Dr. M. K. Wilkinson, and Dr. H. G. Smith for their assistance and hospitality during our stay at Oak Ridge. Some preliminary measurements were performed when one of us (D. L. P.) was a summer visitor at Brookhaven National Laboratory and we are grateful to Dr. J. D. Axe for participating in them. The α-Sn experiment was made possible by Professor A. W. Ewald of Northwestern University, who very kindly provided the crystal. Valuable engineering assistance was provided by R. Kleb. We are also grateful to Dr. G. Dolling of Chalk River Nuclear Laboratories, Canada, for sending a listing of his Coulomb-coefficient program, and to Dr. R. M. Martin and Dr. S. K. Sinha for helpful discussions.

APPENDIX: SHELL-MODEL NOTATION AND EXPRESSIONS FOR DYNAMICAL MATRIX AND ELASTIC AND DIELECTRIC PROPERTIES

We put ion V at (0, 0, 0); ion III at $(-\frac{1}{4}a, -\frac{1}{4}a, -\frac{1}{4}a)$. The charge on ion V is Z_1; charge on ion III is $Z_2 = -Z_1$. First-neighbor force constants between (0, 0, 0) and $(-\frac{1}{4}a, -\frac{1}{4}a, -\frac{1}{4}a)$ are

$$\frac{e^2}{\Omega}\begin{pmatrix}\alpha_x & \beta_x & \beta_x\\ \beta_x & \alpha_x & \beta_x\\ \beta_x & \beta_x & \alpha_x\end{pmatrix};\quad \frac{\beta_x}{\alpha_x}=\gamma_x\,.$$

Second-neighbor force constants between (0, 0, 0) and $(\frac{1}{2}a, \frac{1}{2}a, 0)$ are

$$\frac{e^2}{\Omega}\begin{pmatrix}\mu_x & \nu_x & -\delta_x\\ \nu_x & \mu_x & -\delta_x\\ \delta_x & \delta_x & \lambda_x\end{pmatrix}.$$

Subscript x indicates R(ion-ion), T(ion-shell), or S(shell-shell) interaction. "Atomic" and "mechanical" polarizabilities are π_1, π_2, and d_1, d_2 for the V and III ions, respectively,

$$\pi_i = Y_i^2/(k_i + 4\alpha_T)\,,\quad d_i = -4\alpha_T Y_i/(k_i + 4\alpha_T)\,,$$

where k_i, Y_i are the corresponding core-shell spring constants and shell charges.

Dynamical Matrix

Dynamical matrices $\underline{R}$, $\underline{T}$, and $\underline{S}$ for the three types of short-range interaction are formed from the force constants in the standard way.[54] We define $\underline{M}$, $\underline{Z}$, $\underline{Y}$, and $\underline{k}$ to be diagonal matrices formed from the M_i, Z_i, Y_i, and k_i, respectively, and also

$$\underline{s} = \underline{S} + \underline{k} + (4\alpha_T - 4\alpha_S)\underline{1} .$$

If $\underline{C}$ is the dynamical matrix for Coulomb interactions[58] in a lattice of point charges $|e|$, we define

$$\underline{A} = \underline{R} + \underline{Z}\,\underline{C}\,\underline{Z} ,$$

$$\underline{B} = \underline{T} + \underline{Z}\,\underline{C}\,\underline{Y} ,$$

$$\underline{D} = \underline{s} + \underline{Y}\,\underline{C}\,\underline{Y} .$$

Then the equations of motion for the ions are given by

$$\underline{M}\omega^2\underline{U} = (\underline{A} - \underline{B}\,\underline{D}^{-1}\,\underline{B}^{+})\underline{U} .$$

By definition, $\underline{R}$, $\underline{s}$, and $\underline{C}$ are Hermitian. If assumption (i) (Sec. V) is invoked, so is $\underline{T}$, and thus

$$\underline{B}^{+} = \underline{T} + \underline{Y}\,\underline{C}\,\underline{Z} .$$

Elastic and Dielectric Properties

We now work with the assumptions (i)–(iii) of Sec. V. It is convenient to define further quantities

$$\delta_i = 4\alpha_T/(4\alpha_T + k_i) ,$$

$$\Delta = (\delta_1 + \delta_2 - 2\delta_1\delta_2 S_R)/(1 - S_R^2\delta_1\delta_2) ,$$

$$Z' = Z_1 - \left(\frac{d_2(1 - \delta_1 S_R) - d_1(1 - \delta_2 S_R)}{1 - S_R^2\delta_1\delta_2}\right)$$

(this is the "Szigeti" effective charge),

$$\alpha_R' = \alpha_R(1 - \Delta) ,$$

$$\gamma_R' = \gamma_T + \left(\frac{\gamma_R - \gamma_T}{1 - \Delta}\right)\frac{Z'}{Z_1} .$$

Then the elastic and dielectric properties can be expressed by the following:

$$c_{11} = e^2/a\Omega(\alpha_R + 8\mu_R + 0.247\,62\,Z_1^2) ,$$

$$c_{12} = e^2/a\Omega(-\alpha_R + 2\beta_R - 4\mu_R + 8\nu_R - 4\lambda_R - 2.645\,92\,Z_1^2) ,$$

$$c_{44}^E = e^2/a\Omega[\alpha_R + 4\mu_R + 4\lambda_R + 5.913\,52\,Z_1^2 - \gamma_R^2\alpha_R - (\gamma_R - \gamma_T)^2\alpha_R(\Delta/1 - \Delta) - \tfrac{1}{9}\pi Z_1^2(\epsilon_0 + 2)(\gamma_R' - 2.401\,08)^2] ,$$

$$c_{44}^D = e^2/a\Omega[\alpha_R + 4\mu_R + 4\lambda_R - 3.142\,46\,Z_1^2 - \gamma_R^2\alpha_R - (\gamma_R - \gamma_T)^2\alpha_R(\Delta/1 - \Delta) + \tfrac{1}{9}2\pi Z_1^2(\epsilon_0 + 2)/\epsilon_0(\gamma_R - 1.200\,54)^2] ,$$

$$\alpha_\infty = (\pi_1 + \pi_2 + 2d_1d_2S_R)/(1 - S_R^2\delta_1\delta_2) ,$$

$$\alpha_0 = \alpha_\infty + (Z')^2/4\alpha_R' ,$$

$$\epsilon_{\infty,0} = (1 + \tfrac{8}{3}\pi\alpha_{\infty,0})/(1 - \tfrac{4}{3}\pi\alpha_{\infty,0}),$$

$$\omega_{TO}^2 = (e^2/\overline{M}\Omega)[4\alpha_R' - \tfrac{4}{3}\pi(Z')^2/(1 - \tfrac{4}{3}\pi\alpha_\infty)] ,$$

$$\omega_{LO}^2 = (e^2/\overline{M}\Omega)[4\alpha_R' + \tfrac{8}{3}\pi(Z')^2/(1 + \tfrac{8}{3}\pi\alpha_\infty)] .$$

The last five equations are valid for all diatomic diagonally cubic crystals, and have also been given by Woods, Cochran, and Brockhouse.[59] The piezoelectric constant is[60]

$$e_{14} = (-Z_1 ea/6\Omega)(5.028\,84\,\alpha_0 - \tfrac{1}{2}\gamma_R')(\epsilon_0 + 2) ,$$

and the internal strain parameter[49] is

$$\zeta \equiv -\frac{4\gamma_{14}}{a} = \left(\frac{\gamma_R - \Delta\gamma_T}{1 - \Delta}\right) + \tfrac{1}{3}(\epsilon_0 + 2)\,\frac{\pi Z_1 Z'}{3\alpha_R'}\,(\gamma_R' - 2.401\,08) .$$

Note that when $\gamma_R = \gamma_T$, $\gamma_R' = \gamma_R$ and c_{44}^E and e_{14} reduce to the expressions given by Cowley.[53]

For a rigid-ion model, $\alpha_\infty = 0$ and α_0, c_{44}^E, e_{14}, and ζ simplify to

$$\alpha_0 = Z_1^2/4\alpha_R ,$$

$$c_{44}^E = e^2/a\Omega\{\alpha_R + 4\mu_R + 4\lambda_R - 0.123\,80\,Z_1^2 - \alpha_R\zeta^2[3/(\epsilon_0 + 2)]\} ,$$

$$e_{14} = (Z_1 ea/4\Omega)\,\zeta ,$$

$$\zeta = \tfrac{1}{3}(\epsilon_0 + 2)(\gamma_R - 10.057\,68\,\alpha_0) .$$

---

† Work performed under the auspices of the U. S. Atomic Energy Commission.

[1] C. S. Berry, Phys. Rev. 611, 848 (1967), and references therein.

[2] S. H. Groves and W. Paul, Phys. Rev. Letters 11, 194 (1963).

[3] L. Liu and D. Brust, Phys. Rev. Letters 20, 651 (1968).

[4]D. Sherrington and W. Kohn, Rev. Mod. Phys. 40, 767 (1968); F. Herman, J. Electronics 1, 103 (1965); M. Cardona and D. L. Greenaway, Phys. Rev. 131, 98 (1963).

[5]J. C. Phillips, Phys. Rev. 166, 832 (1968); 168, 905 (1968); 168, 912 (1968); 168, 917 (1968); *Covalent Bonding in Crystals, Molecules and Polymers* (University of Chicago Press, Chicago, 1969).

[6]J. C. Phillips and J. A. Van Vechten, Phys. Rev. Letters 22, 705 (1969).

[7]A preliminary account of the α-Sn results was given by D. L. Price and J. M. Rowe, Solid State Commun. 7, 1433 (1969).

[8]A recent bibliography for these transitions is given by R. W. Keyes, in *Semiconductors and Semi-Metals*, edited by R. K. Willardson and A. C. Beer (Academic, New York, 1968), Vol. 4, p. 327.

[9]J. C. Phillips, Phys. Rev. Letters 20, 550 (1968).

[10]J. C. Phillips, Phys. Rev. Letters 22, 645 (1969).

[11]R. M. Martin, Phys. Rev. Letters 21, 536 (1968); Phys. Rev. 186, 871 (1969).

[12]S. K. Sinha, Phys. Rev. 177, 1256 (1969).

[13]R. M. Pick, M. H. Cohen, and R. M. Martin, Phys. Rev. B 1, 210 (1970).

[14]L. J. Sham, Phys. Rev. 188, 1431 (1969).

[15]R. Banerjee and Y. P. Varshni, Can. J. Phys. 47, 451 (1969), and references therein.

[16]R. M. Martin, Solid State Commun. 8, 799 (1970); Phys. Rev. B 1, 4005 (1970), and references therein; A. W. Solbrig, Jr., and H. L. McMurry in Idaho Nuclear Corporation Report No. IN-1317 Idaho Falls, Ida., 1970, p. 191 (unpublished); B. D. Singh and B. Dayal, Phys. Status Solidi 38, 141 (1970).

[17]A review of these theories is given by B. G. Dick in *Lattice Dynamics*, edited by R. F. Wallis (Pergamon, Oxford, England, 1965), p. 165.

[18]E. Burstein, in *Phonons and Phonon Interactions*, edited by T. A. Bak (Benjamin, New York, 1964), p. 276; M. Lax, in *Lattice Dynamics*, edited by R. F. Wallis (Pergamon, Oxford, England, 1965), p. 179.

[19]W. Cochran, Proc. Roy. Soc. (London) A276, 308 (1963).

[20]W. Cochran, Proc. Roy. Soc. (London) A253, 260 (1959).

[21]G. Dolling, in *Inelastic Scattering of Neutrons in Solids and Liquids* (IAEA, Vienna, 1963), Vol. II, p. 37.

[22]J. L. Warren, R. C. Wenzel and J. L. Yarnell, in *Inelastic Scattering of Neutrons* (IAEA, Vienna, 1965), Vol. I, p. 361; J. L. Warren, J. L. Yarnell, G. Dolling, and R. A. Cowley, Phys. Rev. 158, 805 (1967).

[23]G. Dolling and R. A. Cowley, Proc. Phys. Soc. (London) 88, 463 (1966).

[24]B. N. Brockhouse and P. K. Iyengar, Phys. Rev. 111, 747 (1958); B. N. Brockhouse and B. A. Dasannacharya, Solid State Commun. 1, 205 (1963).

[25]G. Dolling and J. L. Waugh, in *Lattice Dynamics*, edited by R. F. Wallis (Pergamon, Oxford, 1965), p. 19.

[26]J. L. Yarnell, J. L. Warren, and R. G. Wenzel, in *Neutron Inelastic Scattering* (IAEA, Vienna, 1968), Vol. I, p. 301.

[27]A. W. Ewald and O. N. Tufte, J. Appl. Phys. 29, 1007 (1958).

[28]W. Cochran, R. A. Cowley, G. Dolling, and M. M. Elcombe, Proc. Roy. Soc. (London) A293, 433 (1966).

[29]A. Mooradian and G. B. Wright, Phys. Rev. Letters 16, 999 (1966).

[30]M. K. Wilkinson, H. G. Smith, W. C. Koehler, R. M. Nicklow and R. M. Moon, in *Neutron Inelastic Scattering* (IAEA, Vienna, 1968), Vol. II, p. 253.

[31]An interesting discussion of the symmetry of the normal modes in the two structures is given by H. Montgomery, Proc. Roy. Soc. (London) A309, 521 (1968).

[32]These two modes were wrongly labeled in Ref. 7. We are grateful to Dr. A. W. Solbrig, Jr., for bringing this to our attention.

[33]O. Brafman, G. Lengyel, S. S. Mitra, P. J. Gielisse, J. N. Plendl, and L. C. Mansur, Solid State Commun. 6, 523 (1968).

[34]S. Z. Beer, J. F. Jackovitz, D. W. Feldman, and J. H. Parker, Phys. Letters 26A, 331 (1968).

[35]A. Mooradian and G. B. Wright, Solid State Commun. 4, 431 (1966).

[36]A. Pinczuk and E. Burstein, Phys. Rev. Letters 21, 1073 (1968).

[37]R. W. Keyes, J. Appl. Phys. 33, 3371 (1962).

[38]R. E. Lindquist and A. W. Ewald, Phys. Rev. 135, A191 (1964).

[39]L. Liu and E. Tosatti, Phys. Rev. Letters 23, 772 (1969).

[40]J. G. Broerman, Phys. Letters 24, 450 (1970).

[41]G. Dolling, in *Inelastic Scattering of Neutrons* (IAEA, Vienna, 1965), Vol. I. p. 249.

[42]L. J. Slutsky and C. W. Garland, Phys. Rev. 113, 167 (1959), and references therein.

[43]M. Hass, in *Semiconductors and Semi-Metals*, edited by R. K. Willardson and A. C. Beer (Academic, New York, 1967), Vol. 3, p. 3.

[44]M. Hass and B. W. Henvis, J. Phys. Chem. Solids 23, 1099 (1962).

[45]By "high frequency," we mean frequencies high enough so that the ions do not move in response to the electric field but not so high as to cause interband electronic transitions.

[46]F. A. Johnson, Progr. Semicond. 9, 179 (1965).

[47]D. L. Stierwalt, J. Phys. Soc. Japan Suppl. 21, 61 (1966).

[48]G. Arlt and P. Quadflieg, Phys. Status Solidi 25, 323 (1968).

[49]A. Segmüller and H. R. Neyer, Physik Kondensierten Materie 4, 63 (1965).

[50]W. Cochran, Advanc. Phys. 9, 387 (1960); 10, 401 (1961).

[51]J. Pons-Corbeau and J. Jouffroy, Bull. Soc. Franc. Mineral. Crist. XC, 498 (1967).

[52]One can assume this relation for the parameters α without loss of generality, since the ratio of the shell charges is otherwise undefined; this is not the case for the parameters β.

[53]R. A. Cowley, Proc. Roy. Soc. (London) A268, 121 (1962). There are some minor errors in the expressions given in this paper.

[54]M. Born and K. Huang, *Dynamical Theory of Crystal Lattices* (Oxford U. P., Oxford, England, 1954).

[55]Similar expressions have been given by H. Kaplan and J. J. Sullivan, Phys. Rev. 130, 120 (1963). They use a different notation, however, and do not invoke the assumptions (i)–(iii) above.

[56]Reference 25, model *C*(i).

[57]Reference 25, model *C*(ii).

[58]E. W. Kellerman, Phil. Trans. Roy. Soc. London 238, 513 (1940).

[59]A. D. B. Woods, W. Cochran, and B. N. Brockhouse, Phys. Rev. 119, 980 (1960).

[60]The minus sign is put in front of the expression for e_{14} to make it agree with the accepted convention; see D. F. Nelson and E. H. Turner, J. Appl. Phys. 39, 3337 (1968). This convention puts the group-III atom at $(\frac{1}{4}, \frac{1}{4}, \frac{1}{4})$, which is opposite to our definition. The experimental values are negative for all III–V compounds measured so far (see Ref. 48), in contrast to the positive value used for GaAs in Refs. 25 and 55.

PHYSICAL REVIEW B VOLUME 3, NUMBER 4 15 FEBRUARY 1971

Tunable Stimulated Raman Scattering from Mobile Carriers in Semiconductors

C. K. N. Patel and E. D. Shaw
Bell Telephone Laboratories, Murray Hill, New Jersey 07974

(Received 12 August 1970)

In this paper we discuss the recent results of stimulated Raman scattering (SRS) from mobile carriers in semiconductors. Single-particle as well as collective excitations of the electron gas in semiconductors can lead to tunable Raman scattering, which is of considerable interest. We show that some of the possible scattering mechanisms have Raman gain large enough to obtain tunable SRS. The specific case is our recent report of the first observation of tunable SRS in the infrared. This SRS process involves the spin flip of conduction electrons in InSb. Its frequency ω_s is tunable by varying a dc magnetic field B as $\omega_s = \omega_0 - g\mu_B B$, where ω_0 is the frequency of the pump, g is the g value of electrons, and μ_B is the Bohr magneton. With Q-switched CO_2 laser at 10.6 μ as the pump, the spin-flip Raman laser is tunable from 10.9 to 13.0 μ ($B \approx 15$–100 kG). The tunable coherent power is ~ 10 W for an input power of 1.0 kW. The tunable SRS has a linewidth of $\lesssim 0.03$ cm^{-1} at $\omega_s \approx 800$ cm^{-1} and its tuning linearity and resettability exceeds $1 : 3\times10^4$. We will discuss in detail the physics underlying the tunable SRS and describe the possible applications of such a tunable coherent radiation.

I. INTRODUCTION

In this paper we discuss some of the experimental and theoretical results of stimulated Raman scattering (SRS) from conduction electrons in semiconductors. Studies of spontaneous Raman scattering from mobile carriers have shown that both the collective as well as the single-particle processes can give rise to tunable Raman shifts. In Secs. II and III, we evaluate the Raman gains for various scattering processes and show that for some of them, the calculated Raman gain (using the presently available lasers as pump) can be greater than optical losses in the semiconductor, and thus these processes should be eminently suitable for obtaining tunable stimulated Raman scattering.

In Sec. IV, we consider a specific case of the Raman scattering from the Landau level electrons in a semiconductor in a magnetic field, and we describe the experimental results of tunable SRS from spin flip of electrons in n-InSb.[1] The frequency ω_s of the spin-flip Raman laser varies as $\omega_s = \omega_0 - g\mu_B B$, where ω_0 is the pump frequency, g is the effective g value of the conduction electrons, μ_B is the Bohr magneton, and B is the dc magnetic field. Using a Q-switched CO_2 laser at 10.6 μ as the pump, the InSb spin-flip Raman laser can be tuned from ~ 10.9 to 13.0 μ by varying B from ~ 15 to 100 kG. The linewidth of the tunable SRS is $\lesssim 4$ Å at ~ 12.0 μ, corresponding to $\lesssim 0.03$ cm^{-1} at ~ 800 cm^{-1}. The linearity and resettability of SRS frequency exceeds $1 : 3\times10^4$. Both the linewidth and linearity measurements, are, at present, limited by experimental techniques.

With a pump power of ~ 1.0-kW peak, tunable SRS power output is ~ 10 W. In Sec. V we discuss the limitations on the maximum spin-flip Raman laser power output and show that with n-InSb, the maximum power output is limited not by pump depletion but by saturation of the spin system taking into account the spin diffusion.

In Sec. VI, we discuss the tunability limitations of the spin-flip Raman laser and find that for a given electron concentration n-InSb, the lowest magnetic field for SRS is determined by the quantum limit for the upper-spin sublevel, while the upper limit on the magnetic field is determined by the free-carrier absorption. We also discuss the effect of varying the carrier concentration on the spin-flip SRS.

The very narrow linewidth and the extremely linear tunability of the spin-flip Raman laser points to many scientific and practical applications. In Sec. VII, we consider a particular case of infrared spectroscopy and show that the spin-flip Raman laser is superior to the conventional grating spectrometers in terms of resolution and speed.